Dynamic Response Calibration of Sea-Bird Temperature and Conductivity Probes*

MICHAEL C. GREGG

Applied Physics Laboratory and School of Oceanography, University of Washington, Seattle 98105

WILLIAM C. HESS

Applied Physics Laboratory, University of Washington, Seattle 98105

(Manuscript received 31 August 1984, in final form 7 January 1985)

ABSTRACT

Dynamic response calibrations have been made for temperature and conductivity probes produced by Sea-Bird Electronics. These probes are used on wire-lowered and towed conductivity, temperature, and depth systems (CTDs) as well as on free-fall oceanographic profilers. The response of the conductivity cell was measured for free-flow and pumped configurations. Legendre polynomials have been fitted to the measured transfer functions to provide analytic forms for data correction.

1. Introduction

Measurements of oceanic finestructure, i.e., fluctuations with scales between 1 m and about 100 m, are made most easily with sensors that strongly attenuate fluctuations with scales less than 1 m. The conductivity, temperature, and depth (CTD) systems made by Guildline, Meerestechnik-Elektronix and Sea-Bird Electronics (SBE) are in this category. Because the SBE temperature and conductivity sensors are packaged in small self-contained pressure cases, they are also used on a wide variety of towed and free-fall oceanographic vehicles.

The dynamic transfer functions of the SBE sensors have been measured and are reported in this paper to allow investigators to assess the spatial resolution of their data and to develop deconvolution algorithms.

2. Description of the probes

The electronics for both temperature and conductivity sensors are enclosed in small pressure cases attached directly to the sensing elements (Fig. 1). Electrical connectors at the rear of the cases supply voltage and return frequency-modulated output signals. The temperature element is mounted on the front end of the case, inside an open probe guard. The conductivity cell is mounted on the side of the case, enclosed in a solid metal guard. These guards have been removed in Fig. 1 but were in place during the calibrations.

The temperature elements are glass-coated thermistors enclosed in thin-walled steel capillary tubes, which enter the electronics cases through neoprene Morrison seals. This configuration utilizes the high temperature sensitivity of thermistors, yet avoids changes in resistance produced when pressure is applied directly to the beads. Two of the configurations produced by SBE were tested; these are shown in the photograph of Fig. 2a and schematically in Fig. 2b. The lower configuration was used for temperature units with serial numbers 415 through 478; we tested units 417 and 425. The upper design, with a longer steel tube, was used for numbers 479 through 565; we tested numbers 528 and 531. (A number of slow response units are included in the latter sequence of serial numbers. The slow response units have a 6.85-cm-long, 2.1-mm-diameter stainless steel sheath, and our measurements are not applicable.) The longer steel tube was designed to reduce the effect of the thermal mass of the electronics housing on temperature at the probe tip, and hence to improve the dynamic response.

The conductivity cell, shown schematically in Fig. 3, is formed by three electrodes in a Pyrex tube. The length of the glass cell is 19 cm, but the active portion, defined by the separation of the centers of the two outer electrodes, is 12.0 cm long. The diameter is 0.4 cm, yielding a volume of 1.51 cm^3. The outer two electrodes are connected electrically and thus have the same potential and form the sensing volume completely within the cell. The effective electrical resistance is the net resistance of the two regions between the outer and inner electrodes, connected in electrical parallel.

Because normal flushing of the conductivity cell is relatively slow, we connected a pump to the cell to improve its dynamic response. The pump was similar to that supplied by SBE as an accessory with the CTD. This is the configuration in which we have used the

* Contribution Number 1415 of the School of Oceanography, University of Washington.

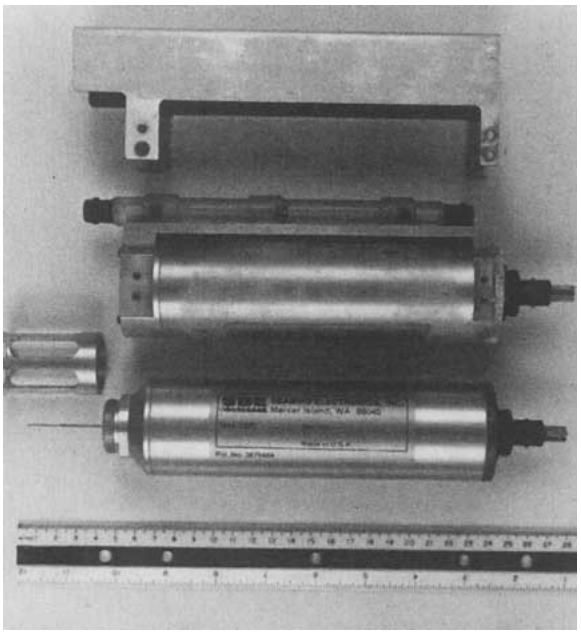

FIG. 1. Temperature probe (bottom) and the conductivity sensor (top). Both units are self-contained; the connector pins at the right supply power and transmit the frequency-modulated output. The sensor guards have been removed to show the sensing elements. A thermistor is located inside the thin tube projecting from the left end of the temperature case. The conductivity cell is the glass (Pyrex) tube mounted on the top of the conductivity case.

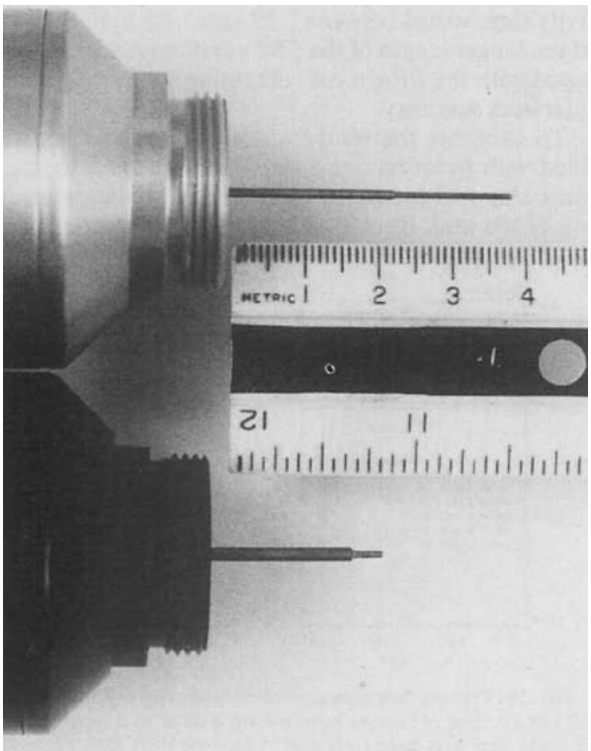

FIG. 2a. Close-up views of the long-tip (upper) and short-tip (lower) temperature probes that were tested.

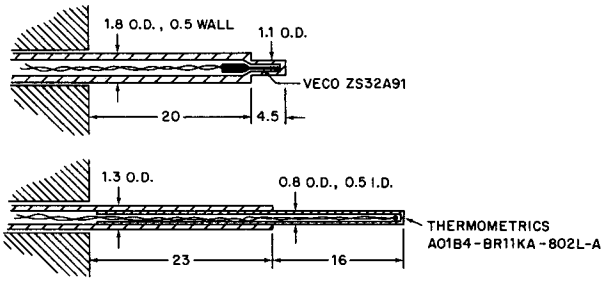

FIG. 2b. Schematic drawings of the two temperature stings. Both consist of thin-walled steel tubes that penetrate a Morrison seal into the electronics case. The probe lengths are in millimeters and the vertical exaggeration of the drawings is 12.5:1.

SBE cells on a towed body, a profiling CTD, and on a free-fall vehicle. No flow irregularities have been observed. The dynamic response tests were run with typical pumping rates (Q = 9 to 30 cm^3 s^{-1}) as well as without the pump connected, which is designated as $Q = 0$.

Both the temperature and the conductivity units are designed with the sensor resistance as one leg of a Wien bridge oscillator circuit. The circuit configurations and static stabilities of the probes have been described previously (Pederson, 1969, 1973; Pederson and Gregg, 1979).

3. Calibration procedure

The procedure was the same used by Gregg *et al.* (1982) to calibrate the Neil Brown conductivity cell: the probes were fired vertically through an interface that had just been sharpened by oscillating stirring grids, and the interface was measured simultaneously with a two-needle reference electrode that had a much finer spatial resolution than the test probes. Signals from the Wien bridge circuits were recorded as voltages, rather than as frequencies, to remove the effect of period counting from the measured transfer functions. These outputs were linear functions of conductivity and temperature to within a few percent. Fourier transforms of the test and reference records were then calculated to form the transfer function of the test probe.

Speeds of 0.25, 0.5, and 1 m s^{-1} were used, which covers the range of velocities of most free-fall profilers

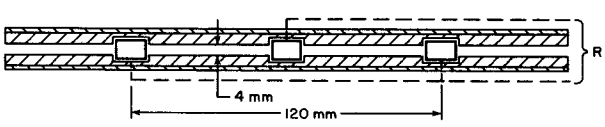

FIG. 3. Schematic drawing of the conductivity cell. The outer two electrodes are connected to hold them at the same potential, so that the net electrical resistance R is formed by the two halves of the cell in parallel.

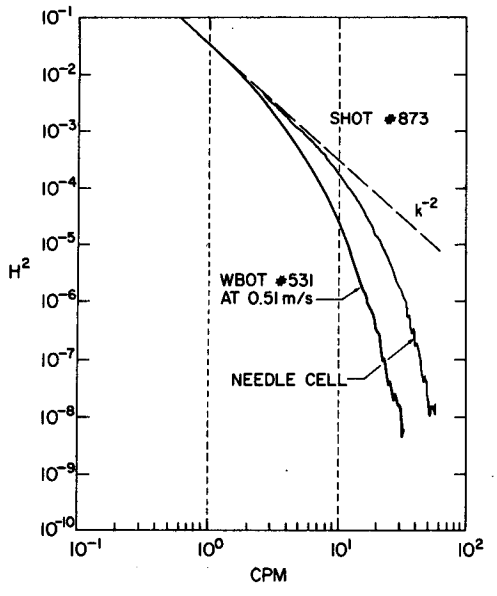

FIG. 4a. Power spectra H^2 of records made with the needle cell and the long temperature probe through a thermally stratified interface. A perfect step would have a spectrum with a k^{-2} behavior. The response of the needle cell is a measure of the thickness of the interface. The wavenumber at which the spectrum of the reference cell is ½ that of the extended k^{-2} line is slightly greater than 10 cpm and is significantly greater than the ½-power attenuation wavenumber of the test cell.

and CTDs used in the ocean. Pumping rates on the conductivity probe were 9, 15, 20, and 30 cm^3 s^{-1}, corresponding to flushing times of 170, 100, 75, and 50 m s^{-1}, respectively, for the active cell volume.

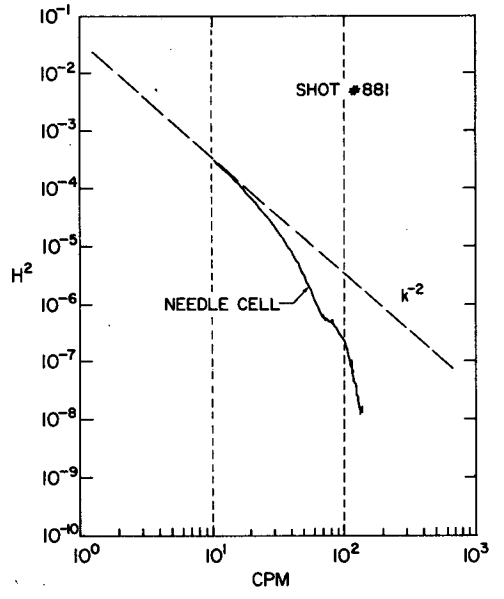

FIG. 4b. Power spectrum of the needle cell through one of the sharper thermally stratified interfaces, with a ½ power wavenumber of 40 cpm.

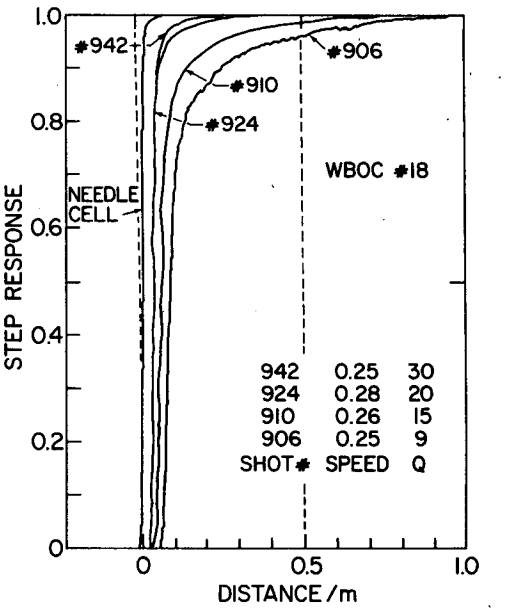

FIG. 5a. Step response curves for the conductivity cell at a speed of 0.25 m s^{-1}, with the reference cell positioned at the leading edge of the test cell. The responses appear complete at distances of 0.3 to 1 m below the interface. The response is dependent on the pumping rate, Q, which is given in cm^3 s^{-1}.

To test the conductivity cells, the calibration tank was filled with two layers of water differing in salinity but maintained at the same temperature. The conductivity steps varied between 2.85 and 5.4 S m^{-1}. Because of the longer length of the SBE conductivity cells compared with the Brown cell, obtaining sufficiently sharp interfaces was easy.

To calibrate the temperature probes the tank was filled with water having a uniform salinity. A temperature step was produced by circulating water near the top of the tank through a heat exchanger and stirring

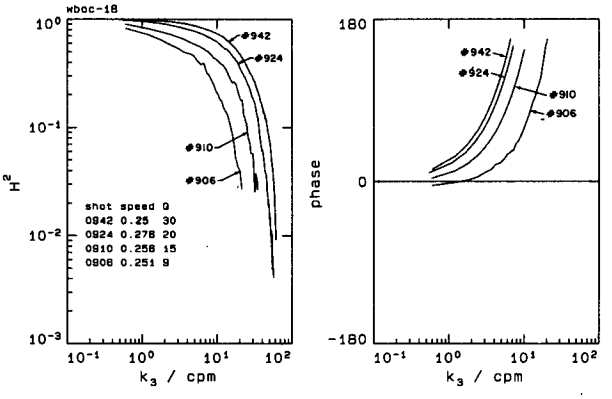

FIG. 5b. Transfer functions for the conductivity cell at a speed of 0.25 m s^{-1}. The H^2 curves have a form similar to a modified sinc function, and have been truncated at wavenumbers higher than the first null. The phase has been computed with respect to the center of the active volume of the cell. Therefore, positive phase angles correspond to a lead in the spatial domain.

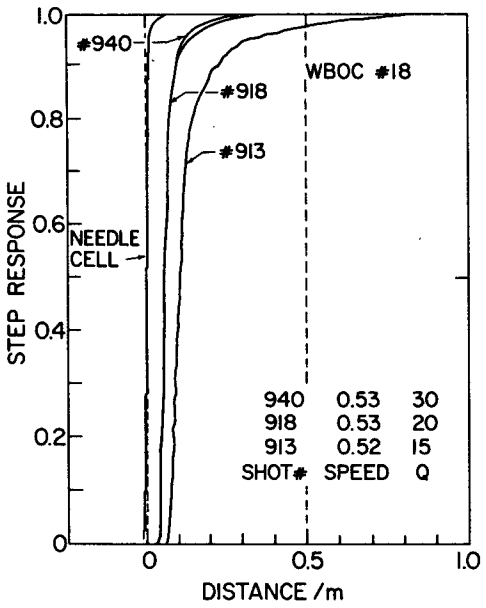

FIG. 6a. Step response curves for the conductivity cell at a speed of 0.5 m s^{-1} with the reference cell positioned at the leading edge of the test cell.

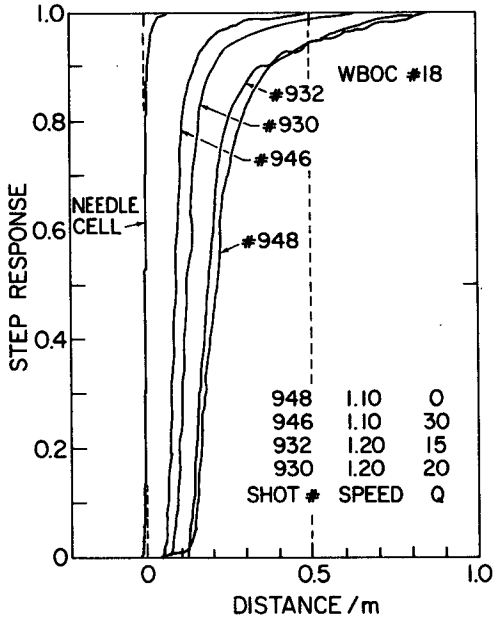

FIG. 7a. Step response curves for the conductivity cell at a speed of 1 m s^{-1}, with the reference cell positioned at the leading edge of the test cell.

gently with slow motions of the grids. Typical temperatures were 20°C in the bottom and 38°C in the top. The much larger diffusivity of heat compared to salt made formation of interfaces more difficult; however, temperature steps sharp enough to calibrate the probes were obtained. Typical examples are shown in Fig. 4a, b. The roll-off of the spectrum of the two-needle cell from the k^{-2} behavior characteristic of step functions is a measure of interface thickness. The interface of shot 873 had a ½-power attenuation, with respect to a k^{-2} behavior, at a wavenumber slightly greater than 10 cycles per meter (cpm) (Fig. 4a), while the ½-power attenuation of the interface in shot 881 was at 40 cpm (Fig. 4b). Both interfaces provided good transfer functions.

4. Response of the conductivity cell

The measured step response curves for the conductivity cell are shown in Figs. 5a, 6a, and 7a for shot speeds of 0.25, 0.5, and 1 m s^{-1}, respectively. Because the reference cell was positioned at the leading edge of the test cell, the initial response of the test cell lags that of the reference cell by several centimeters. Transfer functions, i.e., impulse response functions, corresponding to these curves are shown in Figs. 5b, 6b, and 7b. The phase angle is given with respect to the center of the cell. Hence a positive phase angle corresponds to response of the test cell leading that of the reference positioned at the center of the test cell.

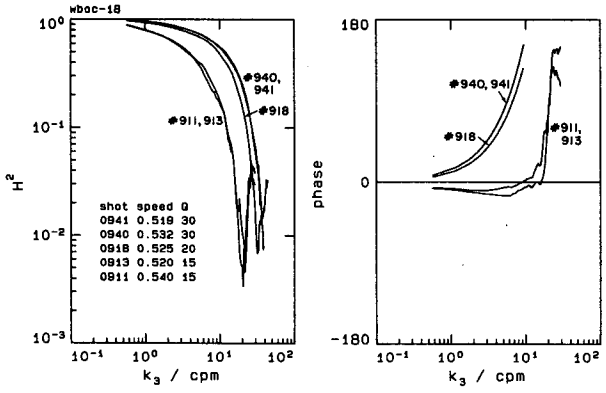

FIG. 6b. Transfer functions for the conductivity cell at a speed of 0.5 m s^{-1}. At 1 cpm $H^2 = 0.98$ for $Q = 20$ and 30 cm^3 s^{-1}, while $H^2 = 0.8$ for $Q = 15$ cm^3 s^{-1}.

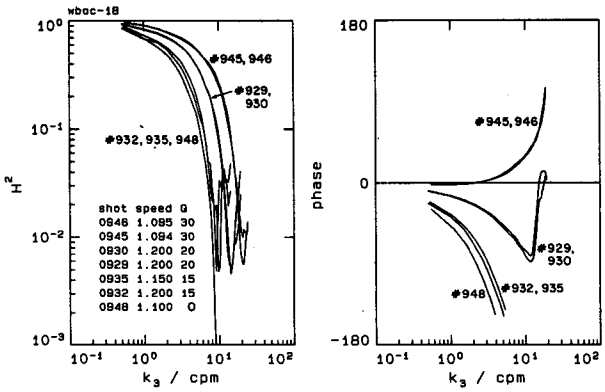

FIG. 7b. Transfer functions for the conductivity cell at a speed of 1 m s^{-1}.

TABLE 1. Effective length of the conductivity cell, in meters, as a function of speed and pumping rate. Entries on the left were determined with Eq. (1); those on the right were determined from the wavenumber of the first null of the transfer function. The actual length is 0.120 m, as shown in Fig. 3. Thus, slow pumping at fast shot speeds can make the effective length greater than the actual length.

	0.25 m s^{-1}	0.5 m s^{-1}	1 m s^{-1}
Q = 30	0.013	0.025	0.050/0.055
Q = 20	0.019	0.038/0.033	0.076/0.076
Q = 15	0.025	0.050/0.049	0.101
Q = 9	0.042/0.039	0.084	0.168

As was the case with the Neil Brown cell, the dominant feature of the amplitude-squared transfer function $H^2(k)$ is the sinc function behavior, where $\text{sinc}(kL) \equiv \sin(\pi kL)/(\pi kL)$, L being the effective length of the cell. Plots of most of the transfer functions have been truncated at wavenumbers slightly greater than the first null. For the Sea-Bird cells

$$L = \frac{1.51U}{Q}\ [\text{m}], \qquad (1)$$

where Q is the pumping rate in cm^3 s^{-1}, and U is the speed in m s^{-1}. Values of L determined from Eq. (1) agree well with those values that could be determined from the position of the first null in the measured transfer functions (Table 1).

In general, the transfer functions show a strong dependence on both speed and pumping rate, with faster responses produced by higher pumping rates. The one exception occurs at speeds of over 1 m s^{-1} where a pumping rate of 15 cm^3 s^{-1} produces essentially the same response as the free-flow condition. We have not attempted to model the hydrodynamics to understand this behavior, but did multiple shots with the same conditions to insure repeatability. The ½-power wavenumbers listed in Table 2 range from 20 to 1.7 cpm. By comparison, the reciprocal of the active length of the cell is 8.3 cpm. Thus, Q = 30 at 0.25 m s^{-1} is an overpumping, but the same pumping rate at 1 m s^{-1} is a slight underpumping. The phase response is determined by: 1) the fact that the interface enters the test cell before it reaches the reference cell, referred to the center of the test cell; and 2) the rate of flow through the test cell. Thus, at a given speed the phase is more positive (or less negative) for higher Q values. For 0.25 m s^{-1} the phase is positive for the pumping rates used, while at 1 m s^{-1} it is positive only for the highest Q values.

TABLE 2. Measured wavenumbers, in cpm, at which H^2 = 0.5 for the conductivity cell. Q is the pumping rate in cm^3 s^{-1}.

	0.25 m s^{-1}	0.5 m s^{-1}	1 m s^{-1}
Q = 30	20	12.5	5.4
Q = 20	14	10.0	3.7
Q = 15	8	3.8	2.2
Q = 9	3		2.0
Q = 0			1.7

Analytic forms for the transfer functions have been obtained by fitting the complex transfer functions $H(k)$ with Legendre polynomials. The measured transfer functions were interpolated with a cubic spline so that they contained at least 500 points, and the fits were constrained to satisfy $H(0)$ = (1, 0). Because the measured functions had several zeros in both the real and imaginary parts, a linear phase was removed prior to fitting. Therefore, the fits had the form

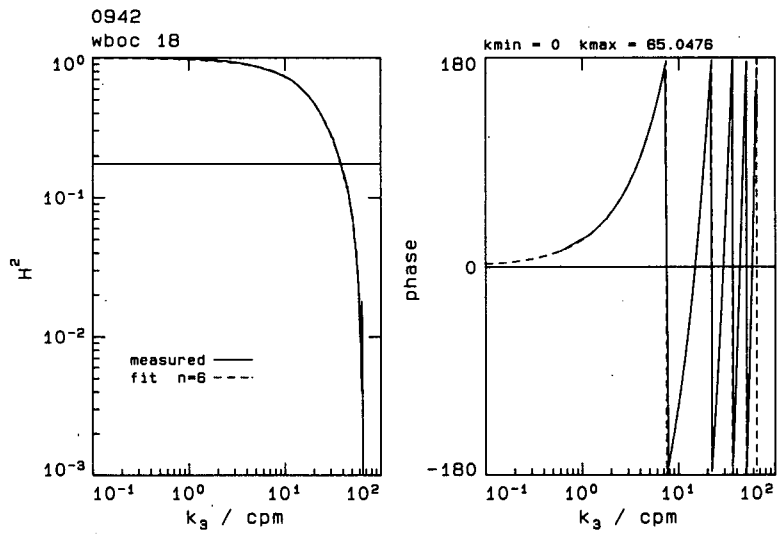

FIG. 8a. Fitted Legendre polynomials (dashed curves) compared with the observed response (solid curves) for shot 942 (0.25 m s^{-1}, Q = 30).

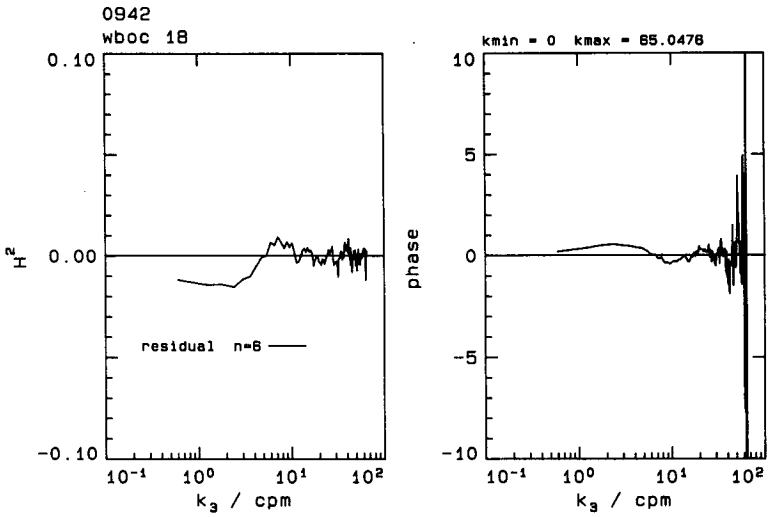

FIG. 8b. Residuals of the fits shown in Fig. 8a.

$$H(k) = e^{2\pi jkl}\{\sum_{n=0}^{M} a_n P_n(2k/k_{\max} - 1)\}, \qquad (2)$$

where the Legendre polynomials are defined by the recursion

$$P_0(x) = 1,$$
$$P_1(x) = x,$$
$$P_n(x) = \{(2n-1)xP_{n-1}(x) - (n-1)P_{n-2}(x)\}/n,$$

with $e^{2\pi jkl}$ as the linear phase term and $j \equiv \sqrt{-1}$.

TABLE 3. Legendre coefficients fitted to the conductivity transfer functions; "l" is the linear offset, or phase length, in meters. For each coefficient the upper value is the real part, and the lower value is the complex part. The speeds and pumping rates of these shots are: shot 906 (0.25, 9); shot 910 (0.26, 15); shot 911 (0.54, 15); shot 918 (0.53, 20); shot 924 (0.28, 20); shot 929 (1.20, 20); shot 932 (1.20, 15); shot 940 (0.53, 30); shot 942 (0.25, 30); shot 945 (1.09, 30); shot 948 (1.10, 0).

Shot	k_{max}	l	a0	a1	a2	a3	a4	a5	a6
0906	24.858	0.02	0.41628	−0.39612	0.077868	−0.039308	0.020463	−0.026091	0.023872
			−0.061172	0.12253	0.040273	−0.055601	0.03631	−0.024243	0.027278
0910	39.945	0.04	0.42081	−0.47772	0.02428	−0.0019825	0.044813	−0.028171	0.0022263
			0.063009	0.11575	−0.063678	−0.039436	0.013707	−0.051041	0.012239
0911	19.742	−0.005	0.42474	−0.46084	0.051605	−0.04823	0.0085136	0.0085082	0.014576
			0.026651	0.11484	−0.064868	−0.058706	0.067602	−0.0148	0.011945
0918	30.202	0.04	0.5411	−0.4448	-5.864×10^{-5}	−0.0014548	0.006586	−0.0018139	0.0043067
			−0.036265	0.079436	0.033708	−0.035921	0.022449	−0.013588	0.010035
0924	54.817	0.06	0.47238	−0.49038	0.022905	0.01054	0.020522	−0.0086046	−0.0042547
			0.029835	0.10608	−0.03264	−0.049234	0.0266	−0.017041	0.01601
0929	14.75	−0.025	0.467	−0.50682	0.012232	−0.0011675	0.0093897	0.0041972	0.007589
			−0.0026636	0.093282	−0.0052122	−0.039181	0.035899	−0.013351	0.012728
0932	10.172	−0.08	0.43382	−0.48208	−0.011962	0.0021949	−0.016295	0.00087194	
			−0.012373	0.12537	-7.2643×10^{-5}	−0.073857	0.019313	−0.028172	0.016472
0940	40.127	0.05	0.47927	−0.47817	0.045319	0.012534	0.0042697	−0.011419	−0.0059086
			−0.13176	0.10115	0.13753	−0.046343	0.012589	−0.015064	0.021389
0942	65.048	0.07	0.50122	−0.47257	0.030224	−0.016357	−0.012321	0.015221	0.0071698
			−0.11539	0.051077	0.053055	−0.061306	0.049457	0.0039786	0.0066314
0945	20.092	0.01	0.50631	−0.47228	0.0035261	−0.0031339	0.028903	0.0002065	−0.013943
			−0.037975	0.097646	0.043244	−0.021249	0.026617	−0.034629	0.0098824
0948	8.8749	−0.1	0.44604	−0.4688	0.05908	−0.02656	0.0040472	−0.0063839	−0.010911
			−0.03929	0.11162	−0.0053485	−0.06288	0.037275	−0.030577	0.025531

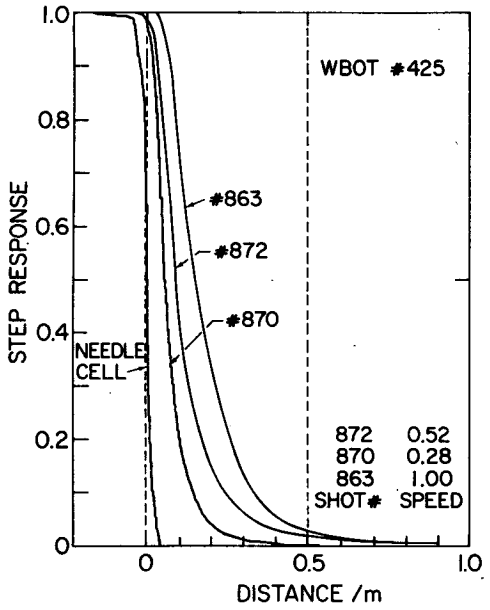

FIG. 9a. Step response curves for the short-tip temperature probe. The response degrades with increasing speed. In all cases the final 5% of the response is very gradual.

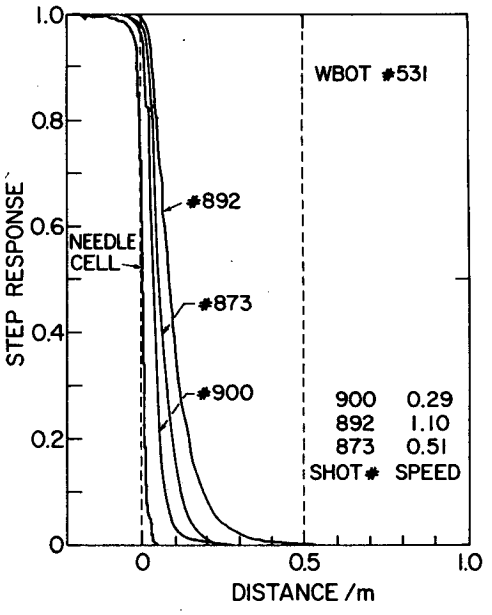

FIG. 10a. Step response curves for the long-tip temperature probe. At all speeds the rise is much faster than for the short-tip probe.

With $M = 6$, fits were obtained with errors of no more than 2% in H^2 and 1° in phase, which is generally better than the reproducibility of the shots. An example is shown in Fig. 8. The polynomial coefficients are given in Table 3.

5. Response of the temperature probes

Step response functions for the temperature probes are shown in Figs. 9a and 10a. A strong speed dependence is evident in both cases. Furthermore, the long probe (Fig. 10a) is significantly faster than the short one (Fig. 9a); at a speed of 1 m s^{-1} the long probe responds completely by ½ m past the interface, but the short probe requires 1 m.

The transfer functions, Figs. 10b and 11b, show the degradation in spatial resolution with increased speed. Both probes provide good resolution to wavenumbers of 1 cpm but not to 10 cpm. As a measure of the resolution, Table 4 contains the wavenumbers and equivalent frequencies of the ½-power point. For the short and long probes, the values range from 3.5 to 1.3 cpm and from 5.6 to 2.2 cpm, respectively. Thus, the ½-power wavenumber of the long probe is about twice that of the short probe. Phase shifts at the ½-power wavenumbers vary between 60 and 70°.

Legendre polynomials in the same form as Eq. (3) give equally good fits to the temperature transfer functions. The coefficients are given in Table 5. As a check, the fitted curves were compared with oceanic temper-

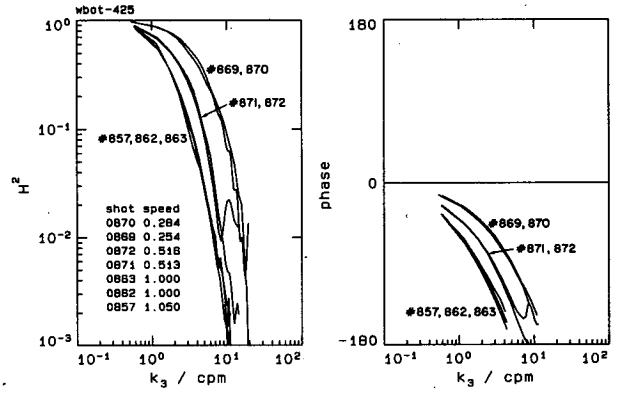

FIG. 9b. Transfer functions for the short-tip temperature probe. At 1 cpm $H^2 = 0.6$–0.9, and the phase shifts are −12 to −31°.

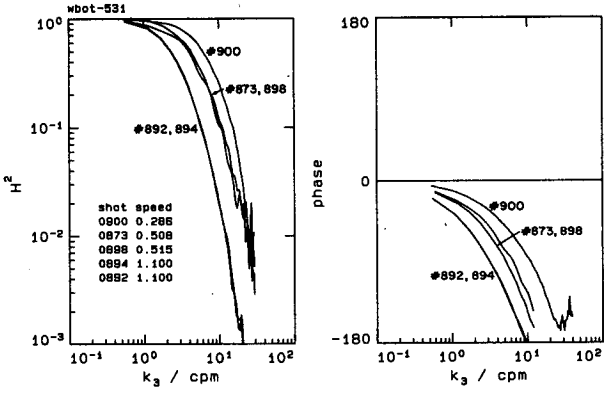

FIG. 10b. Transfer functions for the long-tip temperature probe. At 1 cpm $H^2 = 0.96$–0.83 and the phase is −11 to −37°.

TABLE 4. Wavenumbers and frequencies at which $H^2 = 0.5$ for the temperature probes. For both probes the frequency response improves slightly with faster speed, but the increase is not enough to compensate for the faster speed. Hence, the wavenumber response degrades with speed.

	0.25 m s^{-1}	0.5 m s^{-1}	1 m s^{-1}
Short probe	3.5 cpm (0.88 Hz)	1.8 cpm (0.90 Hz)	1.3 cpm (1.30 Hz)
Long probe	5.6 cpm (1.40 Hz)	3.9 cpm (1.95 Hz)	2.2 cpm (2.20 Hz)

ature data taken simultaneously with an SBE probe and a Fastip thermistor. By using the thermistor as the reference, a transfer function was formed in the same way as with the laboratory data. With this approach it was possible to observe that the Legendre fits agree well with the SBE transfer function over length scales longer than the calibration tank.

6. Comparison of conductivity and temperature responses

To obtain accurate salinity records, the transfer functions of temperature and conductivity should be as closely matched as possible. Differences in response produce "salinity spiking" which becomes severe for significant mismatches. Knowledge of the transfer functions can be used to construct deconvolution algorithms, which we are now developing. A meaningful comparison of the relative merits of the SBE and N. Brown sensors must wait for the deconvolved salinity data produced by both systems. Several points, however, can be made about the best ways to match the SBE sensors.

As evident from Figs. 11 and 12, the H^2 responses are fundamentally different for the SBE conductivity and temperature probes: $H^2(k)$ of the conductivity cell tends to begin rolling off at lower wavenumbers than does the response of the temperature probe, but it also does not roll off as fast for $k > 10$ cpm. This is evident for a speed of 0.25 m s^{-1} in Fig. 11a, but also occurs at higher speeds when the fits are examined at $k < 1$ cpm. The short temperature probe is not well matched with the conductivity probe at any of the speed and pumping configurations examined. Some of these differences may be correctable by deconvolution, e.g., applying a filter that enhances the temperature and conductivity responses to a wavenumber of 2 or 3 cpm and then cuts off both responses at higher wavenumbers.

At 0.25 m s^{-1} the response of the long temperature probe matches that of the conductivity cell for $Q = 20$ at $k < 3$ cpm and for $Q = 9$ at $k > 10$ cpm (Fig. 12a). It is not possible to match over the full wavenumber range. Therefore, the responses should be matched at low wavenumbers by using $Q = 20$; the higher wavenumber data should be smoothed. At faster speeds the long temperature probe is well matched to the conductivity cell with little dependence on pumping rate (Fig. 12c).

Recommendations for optimum use of the SBE cells must wait for development and testing of deconvolution algorithms. The studies we have done show, however, that the most serious salinity spiking is produced by the low wavenumber mismatches in temperature and conductivity responses and that these are worse for no pumping, even if the high wavenumbers appear to be approximately matched. Therefore, we use the long temperature probe and pump the conductivity cell at a rate that depends on the average speed, using the curves in Fig. 12. We recommend this configuration for speeds of 1 m s^{-1} and slower. At faster speeds than

TABLE 5. Legendre coefficients fitted to the transfer functions of the temperature probes; "l" is the linear offset, or phase length, in meters. The upper and lower values for each coefficient are the real and imaginary parts, respectively. For the short temperature probe, the speeds of the shots are: shot 863 (1.00); shot 870 (0.28); shot 871 (0.51). For the long temperature probe, the speeds of the shots are: shot 873 (0.51); shot 894 (1.10); shot 900 (0.29).

Shot	k_{max}	l	a0	a1	a2	a3	a4	a5	a6
0863	7.9189	−0.1	0.33281	−0.44816	0.20556	−0.079742	0.0036399	0.033677	−0.036228
			−0.082858	0.19461	0.0048891	−0.12129	0.095771	−0.044438	0.011074
0870	15.025	−0.03	0.3848	−0.43242	0.19106	−0.056324	−0.011157	0.022673	−0.030774
			−0.22077	0.12599	0.11337	−0.11529	0.072459	−0.033589	0.012052
0871	8.9172	−0.05	0.36118	−0.44332	0.20926	−0.037392	−0.01342	0.022814	−0.014909
			−0.22333	0.14496	0.13151	−0.12484	0.061684	−0.030776	0.019483
0873	19.811	−0.025	0.33205	−0.43095	0.26337	−0.075094	−0.021825	0.047211	−0.032439
			−0.26643	0.13782	0.11535	−0.1563	0.090775	−0.032654	0.0091672
0894	14.952	−0.05	0.30662	−0.41077	0.23025	−0.10999	0.012774	0.030672	−0.039726
			−0.11481	0.20111	0.0096278	−0.12639	0.10019	−0.057048	0.022666
0900	25.035	−0.02	0.45934	−0.47501	0.11713	−0.0084726	−0.021334	0.026892	−0.011735
			−0.068683	0.1081	0.034353	−0.083719	0.056621	−0.0095702	−0.0074784

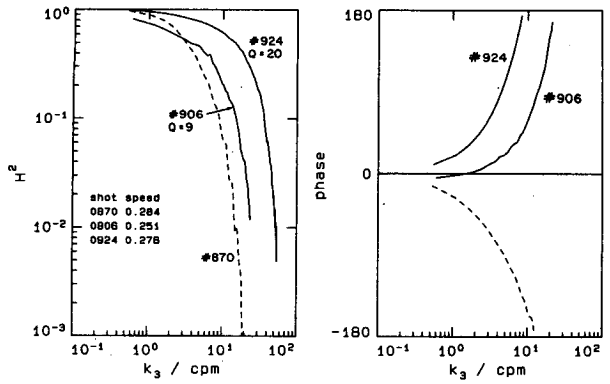

FIG. 11a. Comparison of the transfer functions of the short-tip temperature probe (dashed curve) and those of the conductivity probe at a speed of 0.25 m s^{-1}. The phase comparison is with respect to the center of the conductivity cell.

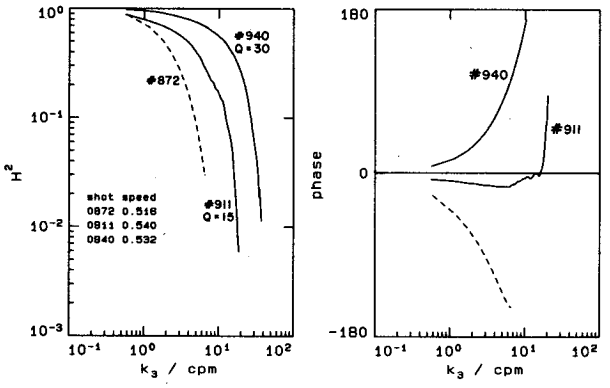

FIG. 11b. Comparison of the transfer functions of the short-tip temperature probe (dashed curve) and those of the conductivity probe at a speed of 0.5 m s^{-1}.

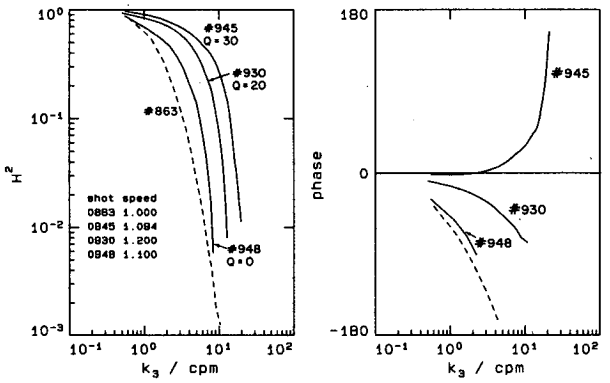

FIG. 11c. Comparison of the transfer functions of the short-tip temperature probe (dashed curve) and those of the conductivity probe at a speed of 1 m s^{-1}.

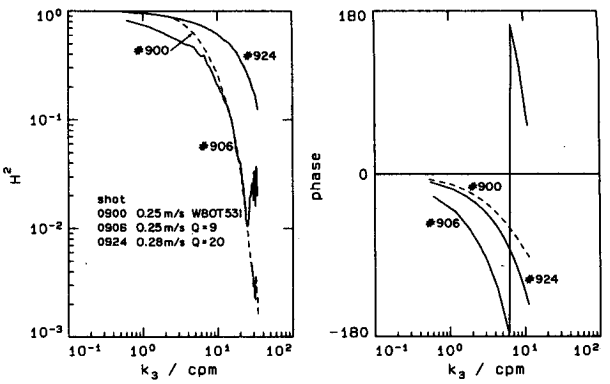

FIG. 12a. Comparison of the transfer functions of the long-tip temperature probe and the conductivity probe at 0.25 m s^{-1}.

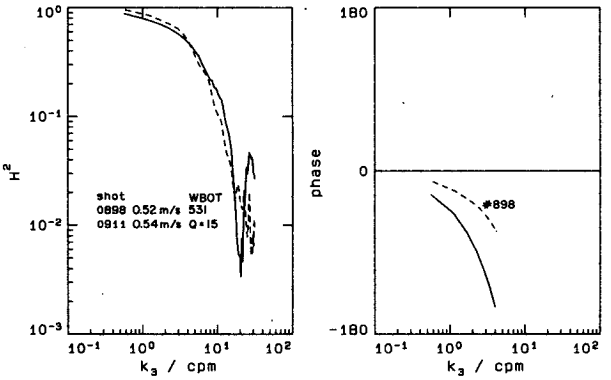

FIG. 12b. Comparison of the transfer functions of the long-tip temperature probe and the conductivity probe at 0.5 m s^{-1}.

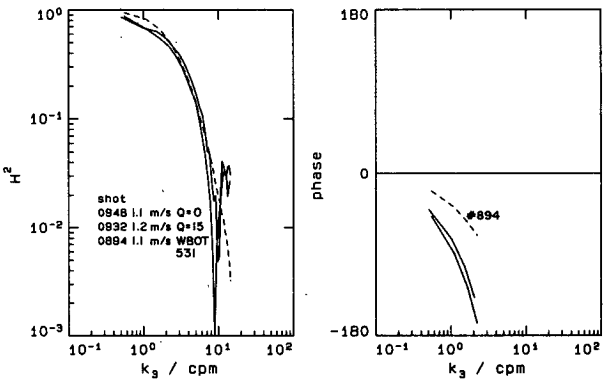

FIG. 12c. Comparison of the transfer functions of the long-tip temperature probe and the conductivity probe at 1 m s^{-1}.

were examined in this study, pumping may not be needed.

Acknowledgments. We are indebted to Earl Krause and Pat McKeown for their skill and dedication in obtaining the shots in the calibration tank, which was funded by the National Science Foundation. These calibrations were funded under contract N00014-80-0252 by the Office of Naval Research as part of the Multi-Scale Profiler program.

REFERENCES

Gregg, M. C., J. C. Schedvin, W. C. Hess and T. B. Meagher, 1982: Dynamic response calibration of the Neil Brown conductivity cell. *J. Phys. Oceanogr.*, **12,** 720–742.

Pederson, A. M., 1969: An accurate low cost temperature sensor. *Trans. Mar. Technol. Soc., Marine Temperature Measurements Symp.*, 135–154.

——, 1973: A small in-situ conductivity instrument. *Oceans 73: 1973 IEEE Int. Conf. on Engineering in the Ocean Environment,* IEEE Publ. 73 CH0774-0 OCC, 68–75.

——, and M. C. Gregg, 1979: Development of a small *in situ* conductivity instrument. *IEEE J. Ocean Eng.*, **OE-4,** 69–75.